View metadata, citation and similar papers at core.ac.uk

brought to you by CORE

provided by DigitalCommons@University of Nebraska

University of Nebraska - Lincoln
DigitalCommons@University of Nebraska - Lincoln

Faculty Publications from the Department of Electrical and Computer Engineering

Electrical & Computer Engineering, Department of

2015

A Discrete-Time Direct-Torque Control for Direct-Drive PMSG-Based Wind Energy Conversion Systems

Zhe Zhang
University of Nebraska-Lincoln, zhang.zhe@huskers.unl.edu

Yue Zhao
Virginia Commonwealth University, Richmond, VA, yzhao3@vcu.edu

Wei Qiao
University of Nebraska-Lincoln, wqiao@engr.unl.edu

Liyan Qu
University of Nebraska-Lincoln, lqu2@unl.edu

Follow this and additional works at: http://digitalcommons.unl.edu/electricalengineeringfacpub

Part of the Computer Engineering Commons, and the Electrical and Computer Engineering Commons

Zhang, Zhe; Zhao, Yue; Qiao, Wei; and Qu, Liyan, "A Discrete-Time Direct-Torque Control for Direct-Drive PMSG-Based Wind Energy Conversion Systems" (2015). *Faculty Publications from the Department of Electrical and Computer Engineering*. 335.
http://digitalcommons.unl.edu/electricalengineeringfacpub/335

This Article is brought to you for free and open access by the Electrical & Computer Engineering, Department of at DigitalCommons@University of Nebraska - Lincoln. It has been accepted for inclusion in Faculty Publications from the Department of Electrical and Computer Engineering by an authorized administrator of DigitalCommons@University of Nebraska - Lincoln.

This article has been accepted for publication in a future issue of this journal, but has not been fully edited. Content may change prior to final publication. Citation information: DOI 10.1109/TIA.2015.2413760, IEEE Transactions on Industry Applications

Industry Applications, IEEE Transactions on
Volume: PP , Issue: 99
DOI: 10.1109/TIA.2015.2413760

A Discrete-Time Direct-Torque Control for Direct-Drive PMSG-Based Wind Energy Conversion Systems

Zhe Zhang, *Student Member*, *IEEE*, Yue Zhao, *Member*, *IEEE*, Wei Qiao, *Senior Member*, *IEEE*, and Liyan Qu, *Member*, *IEEE*

***Abstract*—This paper proposes a novel flux space vector-based direct-torque control (DTC) scheme for permanent magnet synchronous generators (PMSGs) used in variable-speed direct-drive wind energy conversion systems (WECSs). The discrete-time control law, which is derived from the perspective of flux space vectors and load angle, predicts the desired stator flux vector for the next time-step with the torque and stator flux information only. The space-vector modulation (SVM) is then employed to generate the reference voltage vector, leading to a fixed switching frequency as well as lower flux and torque ripples when compared to the conventional DTC. Compared with other SVM-based DTC methods in the literature, the proposed DTC scheme eliminates the use of PI regulators and is less dependent on machine parameters, e.g., stator inductances and permanent-magnet flux linkage, while the main advantages of the DTC, e.g., fast dynamic response and no need of coordinate transform, are preserved. The proposed DTC scheme is applicable for both nonsalient-pole and salient-pole PMSGs. The overall control scheme is simple to implement and is robust to parameter uncertainties and variations of the PMSGs. The effectiveness of the proposed discrete-time DTC scheme is verified by simulation and experimental results on a 180 W salient-pole PMSG and a 2.4-kW nonsalient-pole PMSG used in variable-speed direct-drive WECSs.**

***Index Terms*—Direct torque control (DTC), flux space vector, load angle analysis, permanent-magnet synchronous generator (PMSG), wind energy conversion system (WECS).**

I. Introduction

Over the last two decades, the increasing concerns on energy crisis and environmental pollutions have significantly promoted the utilization of renewable energy. Among various renewable energy sources, wind energy has become one of the most cost-effective sources for electricity generation. The variable-speed wind energy conversion systems (WECSs) which can be operated in the maximum power point tracking (MPPT) mode have attracted considerable interests owing to their high energy production efficiency and low torque spikes [1]. Among different types of generators, the permanent-magnet synchronous generators (PMSGs) have been found superior owing to their advantages such as high power density, high efficiency, and high reliability. Furthermore, a PMSG with a high number of poles can be connected directly to a wind turbine without the use of a gearbox, which significantly reduces the construction, operation, and maintenance costs of the WECSs [2], [3].

Typically, the control systems of PMSGs adopt a decoupled current control executed in a synchronized rotating reference frame. In the last few decades, an alternative electric machine control scheme called the direct torque control (DTC) has attracted extensive attentions from both academia and industry. Different from the decoupled current control, the DTC directly controls electromagnetic torque and stator flux linkage instead of armature currents, hence possessing the merits of fast dynamic response, simple implementation, and high robustness to external disturbances. The DTC has been applied successfully in high-performance industrial servo drive systems [4]. For WECS applications, the DTC may facilitate the realization of MPPT with the optimal torque control [1], since the optimal torque command can be applied directly in the DTC without the need of wind speed measurements. In this way, the outer-loop speed or power controller, which is necessary in the decoupled current control, can be eliminated [5].

In the conventional DTC, the voltage vector commands are determined primarily by the outputs of two hysteresis comparators. Once selected, the desired voltage vector will remain unchanged until the hysteresis states are updated. Although this voltage modulation scheme is simple to execute, it will lead to irregular and unpredictable torque and flux ripples, particularly when the DTC is applied on a digital platform [6]. To solve the problems, many approaches have been developed from different perspectives. One natural thought is to increase the number of available voltage vectors, e.g., using multilevel converters [7], [8] or equally dividing the sampling period into multiple intervals [9]. However,

Manuscript received April 17, 2014; revised September 1, 2014, November 15, 2014 and February 16, 2015; accepted March 1, 2015. This work was supported in part by the U.S. National Science Foundation under grant ECCS-0901218 and CAREER Award ECCS-0954938.

Z. Zhang, W. Qiao and L. Qu are with the Power and Energy Systems Laboratory, Department of Electrical and Computer Engineering, University of Nebraska-Lincoln, Lincoln, NE 68588-0511 USA (e-mail: zhang.zhe@huskers.unl.edu; wqiao@engr.unl.edu; lqu2@unl.edu).

Y. Zhao is with the Department of Electrical and Computer Engineering, Virginia Commonwealth University, Richmond, VA 23284-3072 USA (e-mail: yzhao3@vcu.edu).

0093-9994 (c) 2015 IEEE. Personal use is permitted, but republication/redistribution requires IEEE permission. See http://www.ieee.org/publications_standards/publications/rights/index.html for more information.

This article has been accepted for publication in a future issue of this journal, but has not been fully edited. Content may change prior to final publication. Citation information: DOI 10.1109/TIA.2015.2413760, IEEE Transactions on Industry Applications

these methods will increase the hardware cost, need additional prediction for rotor speed, or have a limited ripple reduction improvement. Another effective technique is to integrate the space-vector modulation (SVM) algorithm into the DTC [10]-[15]. The SVM is able to convert the input voltages into gate signals for the inverter using a fixed switching frequency. A variety of SVM-based DTC schemes have been investigated for permanent-magnet synchronous machines (PMSMs) in the last few decades. In general, they can be classified into two categories based on how the voltage references are generated in the stationary reference frame. In the first category, the decoupled voltage references in the synchronously rotating reference frame are acquired and then transformed to the stationary reference frame using the rotary coordinate transformation [12]-[14]. In the second category, the voltage references are obtained directly from the incremental stator flux vectors in the stationary reference frame without coordinate transformation [15]. Both methods can reduce torque and flux ripples, but need PI controllers to regulate the torque and stator flux errors. The PI gains are usually tuned by a trial and error procedure [12]. Poorly tuned PI gains will deteriorate the dynamic performance of the DTC. In addition, according to [9], a real DTC scheme should not contain PI regulators. More recently, a predictive current control [16], [17] and a deadbeat direct torque and flux control [18] were investigated for surface-mounted and interior PMSMs. These control schemes provide good dynamic performance provided that the information of some machine parameters, e.g., stator inductances and permanent magnet flux linkage, are accurate. Therefore, the performance of the control systems would be more or less influenced by the variations of the machine parameters. Moreover, these control schemes are based on the inverse machine model or a graphical method, which increase the computational complexity.

This paper proposes a discrete-time SVM-based DTC without PI regulators for direct-drive PMSG-based WECSs. The discrete-time control law is derived from the prospective of flux space vectors and load angle. Several machine parameters, e.g., stator inductances and permanent magnet flux linkage, are not presented in the control law. This improves the robustness of the control system to PMSG parameter variations. By adopting the proposed DTC scheme, the torque and flux ripples are reduced and fast dynamic response is retained when compared with the conventional DTC scheme. The proposed DTC scheme is validated by simulation and experimental results for a 2.4-kW nonsalient-pole PMSG and a 180-W salient-pole PMSG used in the direct-drive WECSs.

II. Direct-Drive PMSG-Based Wind Energy Conversion Systems

The configuration of a direct-drive PMSG-based WECS is shown in Fig. 1, where the wind turbine is connected to the PMSG directly without a gearbox. The electrical power generated by the PMSG is transmitted to a power grid or supplied to a load via a variable-frequency power converter.

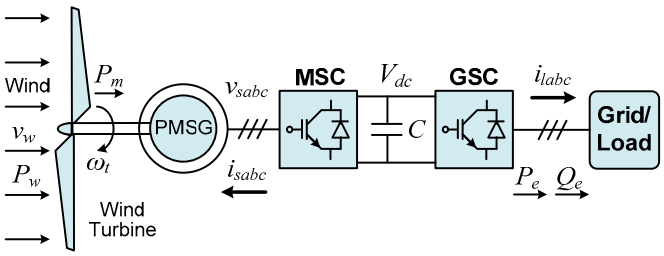

Fig. 1. Configuration of a direct-drive PMSG-based WECS connected to a power grid/load.

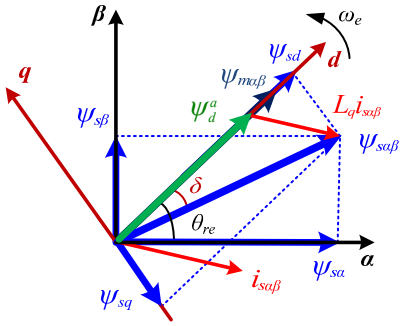

Fig. 2. The space vector diagram of the fluxes and currents of PMSGs.

Typically, the power electronic conversion system consists of a machine-side converter (MSC) and a grid-side converter (GSC) connected back-to-back via a DC link. This paper considers the standard power converter topology in a PMSG-based WECS where both the MSC and the GSC are two-level fully-controlled voltage source converters (VSCs).

A. Wind Turbine Aerodynamic and Shaft Dynamic Models

The mechanical power that can be extracted from wind by a wind turbine is given by:

$$P_m = \frac{1}{2}\rho A_r v_\omega^3 C_p(\lambda) = f(v_\omega, \omega_t), \tag{1}$$

where ρ is the air density; A_r is the area swept by the blades; v_ω is the wind speed; C_P is the turbine power coefficient; ω_t is the turbine shaft speed; and λ is the tip-speed ratio, which is defined by

$$\lambda = \frac{\omega_t r}{v_\omega}, \tag{2}$$

where r is the radius of the wind turbine rotor plane.

As the wind turbine is connected to the PMSG directly, the shaft system of the WECS can be represented by a one-mass model. The motion equation is then given by

$$2H\frac{d\omega_t}{dt} = \frac{P_m}{\omega_t} + \frac{P_e}{\omega_t} - D\omega_t, \tag{3}$$

where $2H$ is the total inertia constant of the WECS, P_e is the electric power generated by the PMSG, and D is the damping coefficient.

B. Modeling of the PMSG

The dynamic equations of a three-phase PMSG can be written in a synchronously rotating dq reference frame (see Fig. 2) as

0093-9994 (c) 2015 IEEE. Personal use is permitted, but republication/redistribution requires IEEE permission. See http://www.ieee.org/publications_standards/publications/rights/index.html for more information.

This article has been accepted for publication in a future issue of this journal, but has not been fully edited. Content may change prior to final publication. Citation information: DOI 10.1109/TIA.2015.2413760, IEEE Transactions on Industry Applications

$$\begin{bmatrix} v_{sd} \\ v_{sq} \end{bmatrix} = \begin{bmatrix} R_s + pL_d & -\omega_e L_q \\ \omega_e L_d & R_s + pL_q \end{bmatrix} \begin{bmatrix} i_{sd} \\ i_{sq} \end{bmatrix} + \begin{bmatrix} 0 \\ \omega_e \psi_m \end{bmatrix}, \quad (4)$$

where p is the derivative operator; v_{sd} and v_{sq} are the d- and q-axis stator terminal voltages, respectively; i_{sd} and i_{sq} are the d- and q-axis stator currents, respectively; R_s is the resistance of the stator windings; L_d and L_q are the d- and q-axis inductances, respectively; ω_e is the rotor electrical angular speed; and ψ_m is the flux linkage generated by the permanent magnets. The d- and q-axis stator flux linkages of the PMSG, ψ_{sd} and ψ_{sq}, have the form of

$$\begin{bmatrix} \psi_{sd} \\ \psi_{sq} \end{bmatrix} = \begin{bmatrix} L_d & 0 \\ 0 & L_q \end{bmatrix} \begin{bmatrix} i_{sd} \\ i_{sq} \end{bmatrix} + \begin{bmatrix} \psi_m \\ 0 \end{bmatrix}. \quad (5)$$

The electromagnetic torque T_e generated by the PMSG can be calculated by

$$T_e = \frac{3}{2} n \cdot \psi_m \cdot i_{sq} + \frac{3}{2} n \left(L_d - L_q \right) i_{sd} \cdot i_{sq}, \quad (6)$$

where n is the number of pole pairs of the PMSG. The torque can also be expressed in terms of stator flux linkage and load angle as follows:

$$T_e = \frac{3}{2} \frac{n}{L_d} |\psi_s| \psi_m \sin\delta + \frac{3}{4} \frac{n}{L_d L_q} |\psi_s|^2 \left(L_d - L_q \right) \sin(2\delta), \quad (7)$$

where $|\psi_s|$ is the magnitude of the stator flux vector and δ is the load angle.

Both of the torque expressions (6) and (7) consist of two terms: the magnetic torque and the reluctance torque. Compared to a nonsalient-pole PMSG ($L_d = L_q$), a salient-pole PMSG can generate a higher torque with the same levels of i_{sd} and i_{sq} owing to the rotor saliency ($L_d \neq L_q$). However, the nonlinear reluctance torque in (7) complicates the mathematical relationship among T_e, $|\psi_s|$ and δ. In [12] and [21], an "active flux" concept was proposed to turn the salient-pole AC machines into nonsalient-pole ones such that the reluctance torque and the magnetic torque were combined as one single term. The active flux magnitude $|\psi_d^a|$ in [12] was defined as

$$|\psi_d^a| = \psi_m + \left(L_d - L_q \right) i_{sd}. \quad (8)$$

The idea can be extended to (7). Substituting i_{sq} from (5) into (6) gives

$$T_e = \frac{3}{2} n \left(\psi_m + \left(L_d - L_q \right) i_{sd} \right) \frac{\psi_{sq}}{L_q}. \quad (9)$$

Since $\psi_{sq} = |\psi_s| \cdot \sin\delta$, the torque in terms of the stator flux magnitude, active flux magnitude, and load angle can be expressed as

$$T_e = \frac{3}{2} \frac{n}{L_q} |\psi_s| |\psi_d^a| \sin\delta. \quad (10)$$

Divide (7) by (10), the active flux magnitude in terms of $|\psi_s|$ and δ has the form of

$$|\psi_d^a| = \frac{L_q}{L_d} \left(\psi_m + \frac{|\psi_s|}{L_q} \left(L_d - L_q \right) \cos\delta \right). \quad (11)$$

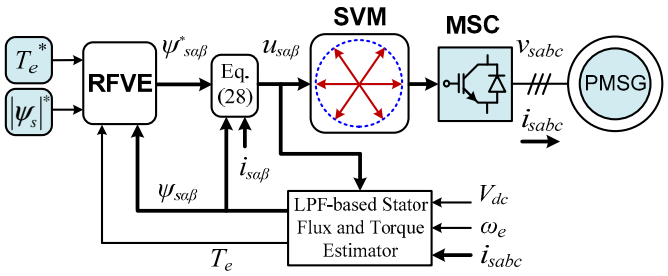

Fig. 3. Schematic of the proposed DTC for a direct-drive PMSG based WECS.

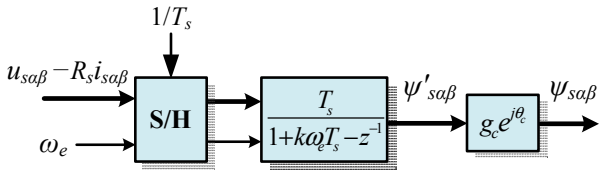

Fig. 4. Discrete-time programmable LPF-based stator flux estimator.

The active flux vector ψ_d^a, which is aligned on the d-axis, can be obtained by

$$\psi_d^a = \psi_{s\alpha\beta} - L_q i_{s\alpha\beta}, \quad (12)$$

where $\psi_{s\alpha\beta}$ and $i_{s\alpha\beta}$ are the stator flux and current vectors in the stationary reference frame, respectively. The diagram in Fig. 2 illustrates the relationship between the fluxes and currents of the PMSG in the vector space, where $\psi_{ma\beta}$ is the rotor flux vector in the stationary reference frame.

III. Proposed Discrete-Time Direct-Torque Control

In the proposed DTC, all the calculations are executed in the stationary $\alpha\beta$ reference frame. The schematic diagram of the proposed DTC is shown in Fig. 3. A reference flux vector estimator (RFVE) is designed to calculate the desired stator flux vector $\psi^*_{s\alpha\beta}$ using the estimated and reference values of the stator flux and electromagnetic torque without PI regulators.

In this paper, the stator flux linkages are estimated by the programmable low-pass filter (LPF) introduced in [19]. To effectively eliminate the DC drift over a wide speed range, the cut-off frequency of the LPF, ω_c, is adjusted according to the rotor electrical speed ω_e by $\omega_c = k \cdot \omega_e$, where k is a constant. The schematic of the discrete-time programmable LPF-based stator flux estimator is shown in Fig. 4. The time derivative term is approximated by the Euler backward differentiation, which is given as

$$s = (1 - z^{-1}) / T_s, \quad (13)$$

where T_s is the sampling period, which is the same as the switching period and control cycle in the proposed DTC. The compensating gain g_c and phase angle θ_c for the output of the LPF are defined as follows

$$g_c = \sqrt{1 + k^2}, \quad (14)$$

$$\theta_c = \frac{\pi}{2} - \tan^{-1}\left(\frac{1}{k} \right). \quad (15)$$

The electromagnetic torque can be calculated as

0093-9994 (c) 2015 IEEE. Personal use is permitted, but republication/redistribution requires IEEE permission. See http://www.ieee.org/publications_standards/publications/rights/index.html for more information.

This article has been accepted for publication in a future issue of this journal, but has not been fully edited. Content may change prior to final publication. Citation information: DOI 10.1109/TIA.2015.2413760, IEEE Transactions on Industry Applications

$$T_e = \frac{3}{2} n(\psi_{s\alpha} i_{s\beta} - \psi_{s\beta} i_{s\alpha}). \quad (16)$$

Compared to (7), the torque expression in (10) is greatly simplified mathematically and can be written as a function of three time-variant variables $|\psi_s|$, $|\psi_d^a|$ and δ. Taking the derivative of (10) on both sides with respect to time yields

$$\frac{dT_e}{dt} = \frac{3}{2}\frac{n}{L_q}|\psi_d^a|\sin\delta \times \frac{d|\psi_s|}{dt} + \frac{3}{2}\frac{n}{L_q}|\psi_s|\sin\delta \times \frac{d|\psi_d^a|}{dt} + \frac{3}{2}\frac{n}{L_q}|\psi_s||\psi_d^a|\cos\delta \times \frac{d\delta}{dt}. \quad (17)$$

The discrete-time form of (17) for a short time interval is given as

$$\Delta T_e = \frac{3}{2}\frac{n}{L_q}|\psi_{d0}^a|\sin\delta_0 \times \Delta|\psi_s| + \frac{3}{2}\frac{n}{L_q}|\psi_{s0}|\sin\delta_0 \times \Delta|\psi_d^a| + \frac{3}{2}\frac{n}{L_q}|\psi_{s0}||\psi_{d0}^a|\cos\delta_0 \times \Delta\delta, \quad (18)$$

where $|\psi_{s0}|$, $|\psi_{d0}^a|$ and δ_0 are the stator flux magnitude, active flux amplitude, and load angle at the reference point, respectively. Equation (18) demonstrates that the flux linkages $|\psi_{s0}|$ and $|\psi_{d0}^a|$ and the loading condition (related to δ_0 and $|\psi_{d0}^a|$) will affect the weights of the flux and load angle increments in the torque increment calculation.

In the kth control step, $|\psi_{s0}| = |\psi_s[k]|$, $|\psi_{d0}^a| = |\psi_d^a[k]|$ and $\delta_0 = \delta[k]$. Then (18) in the discrete-time domain can be written as

$$\Delta T_e[k] = \frac{3}{2}\frac{n}{L_q}|\psi_d^a[k]|\sin\delta[k] \times \Delta|\psi_s[k]| + \frac{3}{2}\frac{n}{L_q}|\psi_s[k]|\sin\delta[k] \times \Delta|\psi_d^a[k]| + \frac{3}{2}\frac{n}{L_q}|\psi_s[k]||\psi_d^a[k]|\cos\delta[k] \times \Delta\delta[k]. \quad (19)$$

The torque $T_e[k]$ has the form of

$$T_e[k] = \frac{3}{2}\frac{n}{L_q}|\psi_s[k]||\psi_d^a[k]|\sin\delta[k]. \quad (20)$$

Dividing (19) by (20) yields

$$\frac{\Delta T_e[k]}{T_e[k]} = \frac{\Delta|\psi_s[k]|}{|\psi_s[k]|} + \frac{\Delta|\psi_d^a[k]|}{|\psi_d^a[k]|} + \frac{\Delta\delta[k]}{\tan\delta[k]}. \quad (21)$$

Then the load angle increment can be derived as

$$\Delta\delta[k] = \tan\delta[k] \times \left(\frac{\Delta T_e[k]}{T_e[k]} - \frac{\Delta|\psi_s[k]|}{|\psi_s[k]|} - \frac{\Delta|\psi_d^a[k]|}{|\psi_d^a[k]|} \right). \quad (22)$$

With the information of the torque reference $T_e^*[k]$ and the reference of the stator flux magnitude $|\psi_s[k]|^*$ as well as the estimated torque $T_e[k]$ and stator flux magnitude $|\psi_s[k]|$ in the kth step, the errors of torque and stator flux magnitude can be calculated as

$$\Delta T_e[k] = T_e^*[k] - T_e[k], \quad (23)$$

$$\Delta|\psi_s[k]| = |\psi_s[k]|^* - |\psi_s[k]|. \quad (24)$$

Substitute (23) and (24) into (22), the increment of load angle in the discrete form can be written as

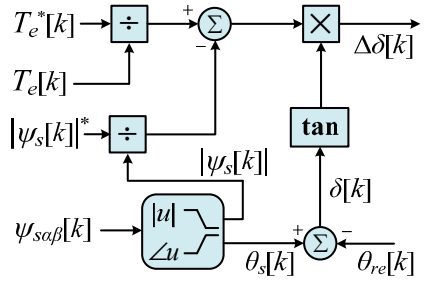

Fig. 5. Block diagram of the load angle increment calculator.

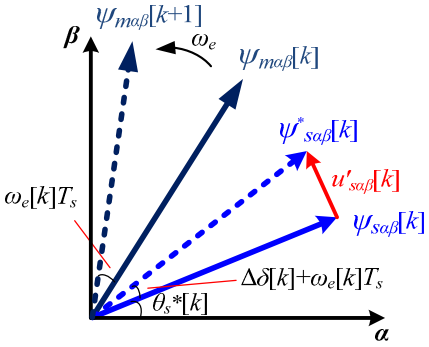

Fig. 6. The voltage vector neglecting the stator resistance in the space vector analysis.

$$\Delta\delta[k] = \tan\delta[k] \times \left(\frac{T_e^*[k]}{T_e[k]} - \frac{|\psi_s[k]|^*}{|\psi_s[k]|} - \frac{\Delta|\psi_d^a[k]|}{|\psi_d^a[k]|} \right), \quad (25)$$

where $\Delta|\psi_d^a[k]|$ is expected to be $|\psi_d^a[k]|^* - |\psi_d^a[k]|$ and $|\psi_d^a[k]|^*$ is the reference of the active flux magnitude in the kth step. The value of $|\psi_d^a|^*$ can be determined from (8) provided i_{sd}^* is known. Based on (4) and (5), the current commands i_{sd}^* and i_{sq}^* can be generated from torque and stator flux commands T_e^* and $|\psi_s|^*$. In practice, to reduce computational burden of the control system, the relation between $|\psi_d^a|^*$ and (T_e^*, $|\psi_s|^*$) can be found offline for different operating conditions based on (4), (5) and (8) and stored in a lookup table for online use.

For a nonsalient-pole PMSG, the active flux $|\psi_d^a|$ is equal to ψ_m so that $\Delta|\psi_d^a[k]|$ is always zero. To simplify the overall control scheme for a salient-pole PMSG, it is assumed the variation of the active flux between two switching cycles is insignificant. In this way, (25) can be simplified as follows for both salient-pole and nonsalient-pole PMSGs

$$\Delta\delta[k] = \tan\delta[k] \times \left(\frac{T_e^*[k]}{T_e[k]} - \frac{|\psi_s[k]|^*}{|\psi_s[k]|} \right). \quad (26)$$

As $|\psi_d^a|$ is a function of $|\psi_s|$ and δ, the steady-state error of $\Delta|\psi_d^a|$ will become zero once $|\psi_s|$ and δ are settled down to their reference values.

Fig. 5 illustrates the block diagram of the algorithm for calculating the load angle increment, where θ_{re} is the electrical rotor position of the PMSG. A small dead band should be set up for $T_e[k]$ and $|\psi_s[k]|$ to avoid a zero denominator. The

0093-9994 (c) 2015 IEEE. Personal use is permitted, but republication/redistribution requires IEEE permission. See http://www.ieee.org/publications_standards/publications/rights/index.html for more information.

This article has been accepted for publication in a future issue of this journal, but has not been fully edited. Content may change prior to final publication. Citation information: DOI 10.1109/TIA.2015.2413760, IEEE Transactions on Industry Applications

reference stator flux angle $\theta_s^*[k]$ can then be obtained from the following equation.

$$\theta_s^*[k] = \Delta\delta[k] + \theta_s[k] + \omega_e[k]T_s. \quad (27)$$

The effect of the rotor speed is taken into consideration by adding the term $\omega_e[k]T_s$ to compensate the rotor position increment when the PMSG operates at a high speed. According to (27) and the magnitude of the desired stator flux linkage $|\psi_s[k]|^*$, the reference stator flux vector in the stationary reference frame, $\psi_{s\alpha\beta}^*[k]$, can be expressed as $\psi_{s\alpha\beta}^*[k] = |\psi_s[k]|^* \cdot e^{j\theta_s^*[k]}$. Then the voltage space vector $u'_{s\alpha\beta}[k]$ neglecting the voltage drop on the stator resistance can be acquired, as shown in Fig. 6. Considering the effect of stator resistance, the expression of the desired stator voltage vector in a discrete-time form can be written as

$$u_{s\alpha\beta}[k] = \frac{\psi_{s\alpha\beta}^*[k] - \psi_{s\alpha\beta}[k]}{T_s} + R_s i_{s\alpha\beta}[k]. \quad (28)$$

When implementing the proposed discrete-time DTC, the criterion $dT_e/d\delta > 0$ should be always met to ensure the stability of the direct torque controlled PMSG systems. According to this stability criterion, the maximum load angle for a salient-pole PMSG is

$$\delta_{\max} = \arccos\left(\frac{b - \sqrt{b^2 + 8a^2}}{4a}\right), \quad a = \frac{L_q - L_d}{L_q}, b = \frac{\psi_m}{|\psi_s|}. \quad (29)$$

The derivation of (29) is provided in Appendix. With the knowledge of $u_{s\alpha\beta}[k]$, proper switching signals can be generated by the SVM module to achieve fast, accurate torque and flux linkage control.

IV. Simulation Results

A. System Setup Description

Simulation studies are carried out in MATLAB/Simulink to validate the proposed discrete-time DTC scheme for two PMSGs. The parameters of the two PMSGs are listed in Table I. The power rating of the salient-pole PMSG #1 is 180 W and its DC-bus voltage is 41.75 V. The nonsalient-pole PMSG #2 is used in a practical direct-drive WECS (Skystream 3.7) with a 2.4-kW rated power and DC-bus voltage of 300 V. In the simulation, the value of k in (14) and (15) is set as $1/\sqrt{2}$. The sampling period is 100 μs for both PMSG control systems, which is typically equal to one PWM control cycle in practical applications. The dead-time of the IGBTs in the MSC is set as 1 μs and is compensated by the algorithm introduced in [22].

B. Validation of the Proposed DTC on PMSG #1

The performance comparison of the proposed DTC, the conventional DTC, and a stator flux-oriented SVM-DTC (named PI-DTC) in [12] is firstly investigated on PMSG #1. The conventional DTC in this paper is implemented by adopting the switching table in [10], where the torque error is regulated by a three-level torque hysteresis controller. The stator flux is estimated by using the PMSG current model in the stationary reference frame, which is given by

Table I. Parameters of the PMSGs

Parameter	PMSG #1	PMSG #2
Number of pole pairs p	4	21
Magnet flux linkage ψ_m	0.01344 V·s	0.2532 V·s
Stator resistance R_s	0.235 Ω	1.5 Ω
d-axis inductance L_d	0.275 mH	0.87 mH
q-axis inductance L_q	0.364 mH	0.91 mH

$$\begin{bmatrix}\psi_{s\alpha}\\ \psi_{s\beta}\end{bmatrix} = \begin{bmatrix}L + \Delta L\cos(2\theta_{re}) & \Delta L\sin(2\theta_{re})\\ \Delta L\sin(2\theta_{re}) & L - \Delta L\cos(2\theta_{re})\end{bmatrix}\begin{bmatrix}i_{s\alpha}\\ i_{s\beta}\end{bmatrix} + \psi_m\begin{bmatrix}\cos\theta_{re}\\ \sin\theta_{re}\end{bmatrix}, \quad (30)$$

where $L = (L_d + L_q)/2$ and $\Delta L = (L_d - L_q)/2$. The current model-based stator flux estimator could achieve good performance in both steady and transient states, but needs more machine parameters compared to the voltage model-based stator flux estimator used in the proposed DTC.

In this test, the speed of the PMSG #1 is kept at 1500 RPM; the torque reference is −0.1 N·m from the beginning, and then is decreased to −0.5 N·m at 0.025 s; the command of the stator flux magnitude is 0.0135 V·s at the beginning and then is decreased to 0.013 V·s at 0.025 s; and both reference variations are step changes. In the conventional DTC, the torque and stator flux hysteresis bandwidths are set as 0.2 N·m and 0.0003 V·s, respectively. The PI gains of the PI-DTC are tuned carefully to achieve good control performance for PMSG #1. Fig. 7 compares the torque, stator flux magnitude, and instantaneous phase-A stator current of PMSG #1 controlled by the conventional DTC, the PI-DTC, and the proposed DTC with a 10 kHz sampling frequency as well as by the conventional DTC with a 67 kHz sampling frequency (named DTC-1). The switching behavior of the conventional DTC determines that its switching frequency is lower than the SVM-DTCs when using the same sampling frequency [14]. Thus, in the DTC-1 case, the sampling frequency of the conventional DTC is increased to 67 kHz to obtain an equivalent switching frequency of 10 kHz, which is obtained by calculating the average turning-on/off frequency of an inverter leg within 0.05 s [23]. As shown in Fig. 7, the maximum peak-to-peak torque ripples of the conventional DTC, the PI-DTC, the proposed DTC and the DTC-1 are 1.2 N·m, 0.1 N·m, 0.1 N·m and 0.33 N·m, respectively; and the maximum peak-to-peak ripples of the stator flux magnitudes in the four cases are 0.008 V·s, 0.0004 V·s, 0.0004 V·s and 0.0012 V·s, respectively. The stator currents controlled by the PI-DTC and the proposed DTC are much smoother with less harmonic contents than those controlled by the conventional DTC and DTC-1. Thus, compared with the conventional DTC, the SVM-DTCs (including the proposed DTC and the PI-DTC) showed a distinct superiority in reducing the steady-state torque and stator flux magnitude ripples and stator current harmonics for different loading conditions. This is true even when the conventional DTC is implemented with a much higher sampling frequency (leading to a higher computational cost) so as to have an equivalent switching frequency same as

0093-9994 (c) 2015 IEEE. Personal use is permitted, but republication/redistribution requires IEEE permission. See http://www.ieee.org/publications_standards/publications/rights/index.html for more information.

This article has been accepted for publication in a future issue of this journal, but has not been fully edited. Content may change prior to final publication. Citation information: DOI 10.1109/TIA.2015.2413760, IEEE Transactions on Industry Applications

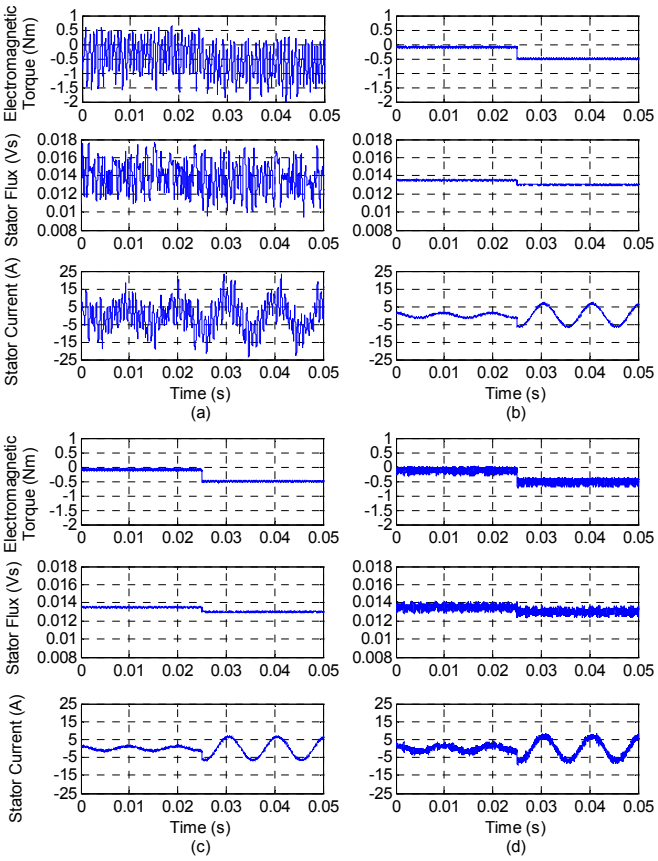

Fig. 7. The dynamic responses of torque, stator flux magnitude, and instantaneous phase-A stator current of PMSG #1 using (a) the conventional DTC, (b) the PI-DTC, and (c) the proposed DTC with a 10 kHz sampling frequency as well as (d) the conventional DTC with a 67 kHz sampling frequency (DTC-1).

the switching frequency of the proposed DTC and the PI-DTC.

The tracking performance of the proposed DTC is shown in Fig. 8. In this test, the PMSG #1 is operated at 2000 RPM, and the torque command is step changed from −0.2 N·m to −0.5 N·m at 3×10^{-4} s. The references of the stator flux and active flux magnitudes are calculated based on the maximum torque per ampere (MTPA) curve. The dynamics of the torque angle increment (top) and the torque (bottom) with/without active flux compensation are compared in Fig. 8. The active flux term does not affect the dynamic performance of the proposed DTC, which proves the feasibility of the assumption (26). The torque is capable of tracking its command within two switching cycles.

The proposed DTC is also tested with various parameter variations, where the operating condition of the PMSG is the same as that in Fig. 8. Fig. 9 shows the percentage torque errors with respect to the values in Fig. 8 when the rotor magnet flux linkage or the *d*- and *q*-axis inductances change while all other parameters of the machine are kept at the nominal values. Fig. 9 (left) shows the cases when the rotor magnet flux linkage has a: 1) 10% decrease without considering the active flux, i.e. using (26); 2) 10% decrease while considering the active flux, i.e., using (25); 3) 10% increase without considering the active flux; and 4) 10% increase while considering the active flux. Fig. 9 (right) shows the cases when both the *d*- and *q*-axis inductances have: 1) 20% decrease without considering the active flux; 2) 20% decrease while considering the active flux; 3) 20% increase without considering the active flux; and 4) 20% increase while considering the active flux. From the results in Fig. 9, the percentages of the torque error are no more than 2% of the torque values in Fig. 8 in all of the cases; and the torque errors

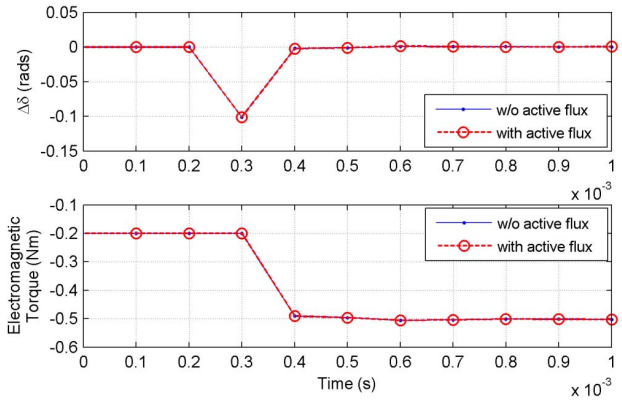

Fig. 8. The dynamic responses of the torque angle increment (top) and the electromagnetic torque (bottom) under a step torque change for PMSG #1.

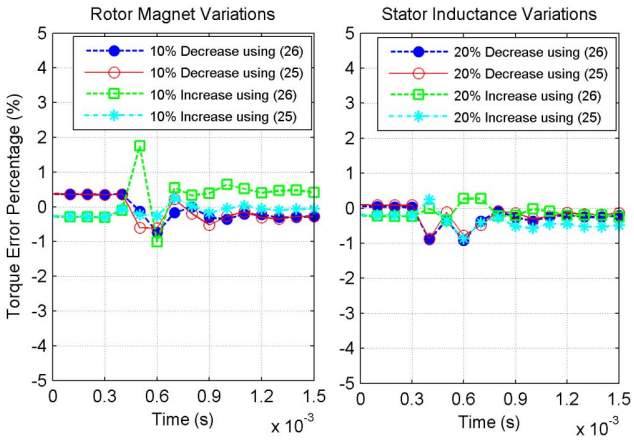

Fig. 9. The torque errors in percentage with respect to the results in Fig. 8 when the rotor magnet flux linkage (left) or the stator inductances (right) vary.

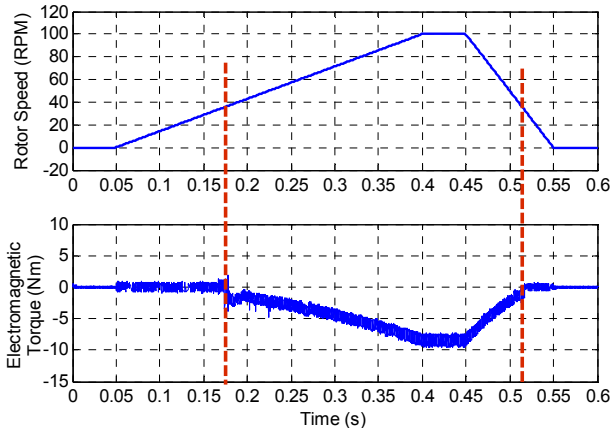

Fig. 10. The rotor speed and torque responses of PMSG #2 during the startup and low-speed operating conditions.

0093-9994 (c) 2015 IEEE. Personal use is permitted, but republication/redistribution requires IEEE permission. See http://www.ieee.org/publications_standards/publications/rights/index.html for more information.

This article has been accepted for publication in a future issue of this journal, but has not been fully edited. Content may change prior to final publication. Citation information: DOI 10.1109/TIA.2015.2413760, IEEE Transactions on Industry Applications

are always damped to almost zero within 8 cycles. Therefore, the proposed DTC can achieve a fast dynamic response and its robustness to machine parameter variations is proven.

C. Validation of the Proposed DTC on PMSG #2

The startup behavior and low speed performance of the proposed DTC are evaluated on PMSG #2. Since the inputs of the low-pass filter-based stator flux estimator at zero speed are null, the estimator is ineffective during the wind turbine startup. To solve the problem, a supplementary *V/f* control is used to assist the operation of the proposed DTC during the startup process and very low speed condition. The ratio of voltage to frequency is chosen to make the output power of the PMSG equal to zero. The control algorithm will be switched from the *V/f* control to the proposed DTC with MPPT if the rotor speed exceeds 33 RPM (11% of the rated speed). In this test, the rotating speed of the PMSG is zero at the beginning, then is increased to 100 RPM from 0.05 s to 0.4 s, and finally decreases to zero from 0.45 s to 0.55 s. As shown in Fig. 10, the proposed DTC-based MPPT is activated quickly when the rotor speed increases to 33 RPM and switches to the *V/f* control quickly when the rotor speed decreases to 33 RPM; the torque response during the transitions is smooth. The results show that with the aid of the *V/f* control, the proposed control scheme can cover the entire operating range of the WECS.

The proposed DTC is also applied on PMSG #2 to simulate the operation of a real WECS. The parameters of the wind turbine are given as follows. The radius of the blades is R = 1.86 m; the swept area is 10.87 m^2; the air density is ρ = 1.15 kg/m^3; the equivalent damping coefficient of the shaft system is D = 0.001; the turbine power coefficient $C_p(\lambda)$ is evaluated as follows:

$$C_P = 1.11 \cdot (9.67 - \lambda) \exp(0.261\lambda - 3.05) - 0.5083, \quad (31)$$

where C_P reaches the maximum value of 0.4169 when λ equals to 5.84. The total momentum of inertia of the WECS is 0.08 kg·m^2. The GSC is connected to a three-phase ideal source. Its phase-to-phase RMS voltage is 190.5 V. The line impedance is 1 mH and the DC link capacitance is 11.2 mF. The GSC is controlled by the vector control scheme in [24]. A randomly generated 10-second wind speed profile is used for the simulation study, as shown in Fig. 11(a). The wind speed varies in the range of ±2 m/s around the mean value of 7.5 m/s. The torque command for the MPPT is given as [20]

$$T_e^* = K_{opt}\omega_t^2, \quad (32)$$

where K_{opt} is a constant determined by the wind turbine characteristics, which is equal to 0.0843 for the wind turbine used in this study. The stator flux magnitude command is obtained from the torque command based on the principle of MTPA to enhance the efficiency of the PMSG. The dynamic responses of the shaft speed, the actual and optimal power coefficients, the estimated and reference torques, and the DC bus voltage during wind speed variations are shown in Figs. 11(b), (c), (d), and (e), respectively. The shaft speed of the WECS follows the wind speed profile closely so as to capture

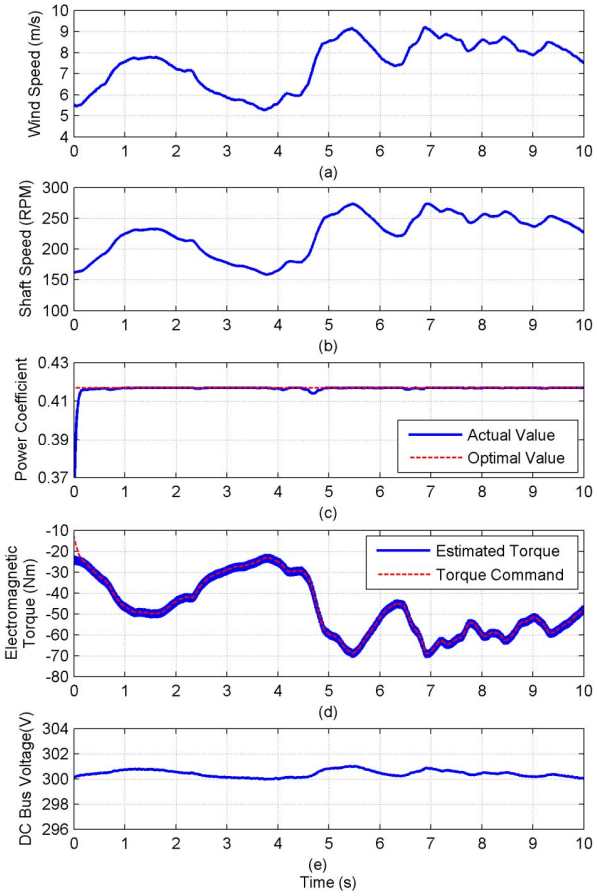

Fig. 11. The dynamic performance of the PMSG #2-based direct-drive WECS controlled by the proposed DTC under variable wind speed conditions: (a) wind speed, (b) shaft speed, (c) actual and optimal power coefficients, (d) electromagnetic torque and its command, and (e) DC bus voltage.

the maximum energy from the wind. As Fig. 11(c) shows, the actual power coefficient approaches its optimal value with the deviations less than 0.003. With the proposed DTC, the electromagnetic torque of the PMSG is controlled directly and quickly. The estimated torque and its command are on top of each other. The maximum peak-to-peak torque ripple is 4 N·m, which is 5% of the rated torque of the PMSG. The DC bus voltage is fluctuated between 299.9V and 301V but has little effect on the torque tracking performance. Therefore, by using the proposed DTC and the optimal torque command calculated from (32), the MPPT of the wind turbine can be achieved quickly and reliably by using one torque control loop without the need of wind speed information.

V. Experimental Results

Experimental studies are carried out to further validate the performance of the proposed DTC scheme for the PMSGs listed in Table I. Fig. 12(a) illustrates the schematic of the experimental system setup for PMSG #1. A DC motor is operated as the prime mover, which is powered by a DC source through a full-bridge DC-DC converter. The power generated by the PMSG is sent back to the DC bus via a three-phase converter. The PMSG and the DC motor are connected through a mechanical coupling. The control algorithms are

0093-9994 (c) 2015 IEEE. Personal use is permitted, but republication/redistribution requires IEEE permission. See http://www.ieee.org/publications_standards/publications/rights/index.html for more information.

This article has been accepted for publication in a future issue of this journal, but has not been fully edited. Content may change prior to final publication. Citation information: DOI 10.1109/TIA.2015.2413760, IEEE Transactions on Industry Applications

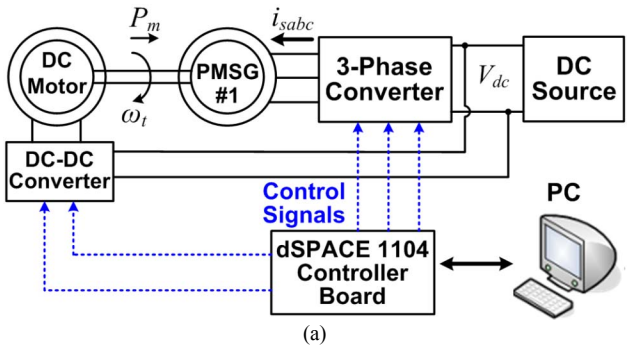

(a)

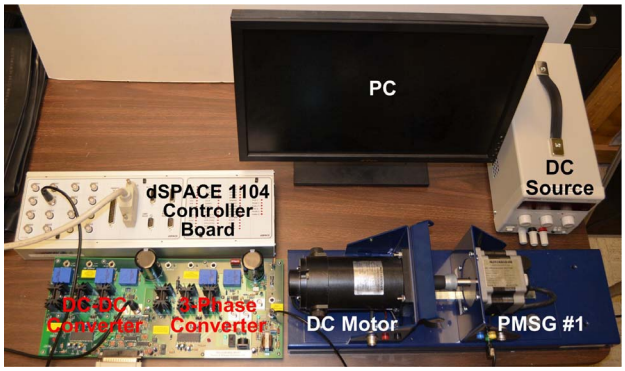

(b)

Fig. 12. The experimental setup for PMSG #1: (a) the schematic and (b) the real experimental system setup.

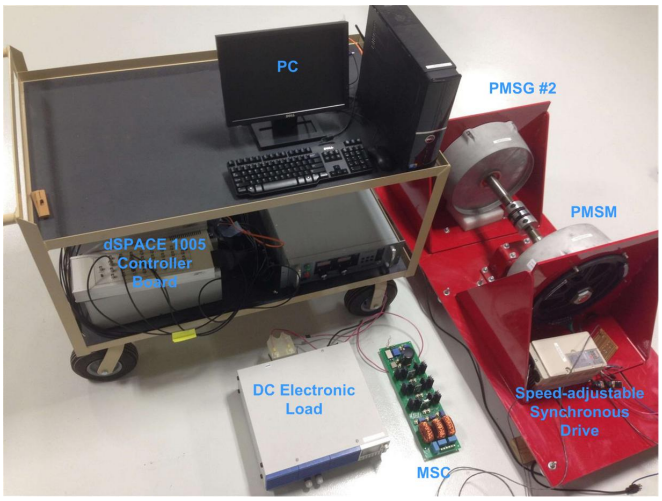

Fig. 13. The experimental system setup for PMSG #2.

implemented on a dSPACE 1104 controller board. Fig. 12(b) shows the real experimental system setup. The real experimental system setup for PMSG #2 is shown in Fig. 13, where a speed-adjustable PMSM (same as PMSG #2) drive is employed to emulate the dynamics of the wind turbine to drive the PMSG directly. The AC power generated by the PMSG is converted to DC power by a three-phase IGBT converter (i.e., the MSC). A DC electronic load is utilized to stabilize the DC-terminal voltage of the MSC and consume the power generated by the PMSG. The control algorithms are implemented on a dSPACE 1105 controller board. The control algorithms are executed with a sampling period of 100 μs, which is the same as the SVM switching frequency. The dead-time compensation scheme is the same as that used in

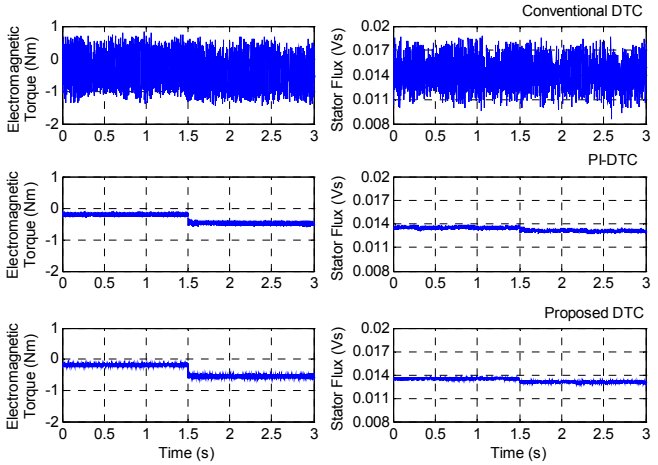

Fig. 14. The dynamic responses of torque and stator flux magnitude of PMSG #1 controlled by the conventional DTC, the PI-DTC, and the proposed DTC.

simulation studies. All of the experimental results are recorded using the ControlDesk interfaced with dSPACE 1104/1005 and a laboratory computer (PC).

The steady-state and dynamic performances of the conventional DTC, the PI-DTC, and the proposed DTC are compared using PMSG #1 in Fig. 14. Due to the physical limits of the dSPACE control system, e.g., the analog/digital conversion (ADC) sampling rate, the processor speed, etc., the sampling frequency is set as 10 kHz. The PMSG #1 is operated at 1500 RPM. The boundaries of the hysteresis controllers for the conventional DTC are the same as those in the simulation. The commands of torque and stator flux magnitude start from −0.2 N·m and 0.0135 V·s, then change to −0.5 N·m and 0.013 V·s at 1.5 s, respectively. Both reference variations are step changes. The PI gains of the PI-DTC are well tuned such that the PI-DTC achieves the same steady-state performance and transient response as the proposed DTC for this test. With the conventional DTC, the maximum peak-to-peak torque and stator flux magnitude ripples are 1.8 N·m and 0.009 V·s, respectively. However, when the PI-DTC and the proposed DTC are used, the maximum peak-to-peak torque and stator flux magnitude ripples decrease to 0.16 N·m and 0.0005 V·s, respectively. Therefore, the integration of the SVM in the DTC can significantly reduce the torque and stator flux magnitude ripples of PMSGs.

The steady-state and transient performances of PMSG #2 with the proposed discrete-time DTC scheme are shown in Fig. 15. In the experiment, the rotor speed is kept at 180 RPM and the reference of the stator flux magnitude is 0.2532 V·s. The torque command is −10 N·m at the beginning, then increased to −30 N·m at 3 s, and finally decreased to −20 N·m at 8 s. Both torque command variations are step changes. The estimated electromagnetic torque follows its command quickly and closely. The torque ripples are within the range of [-2, 2] N·m, which are no more than ±3% of the rated torque. The stator flux magnitude estimated by the LPF is always around 0.2532 V·s with the maximum ripples of ±0.0003 V·s (0.12% of the rated stator flux). Therefore, the advantages of the proposed DTC, e.g., fast dynamic response and low torque and flux ripples in the steady-state operation, are verified.

0093-9994 (c) 2015 IEEE. Personal use is permitted, but republication/redistribution requires IEEE permission. See http://www.ieee.org/publications_standards/publications/rights/index.html for more information.

This article has been accepted for publication in a future issue of this journal, but has not been fully edited. Content may change prior to final publication. Citation information: DOI 10.1109/TIA.2015.2413760, IEEE Transactions on Industry Applications

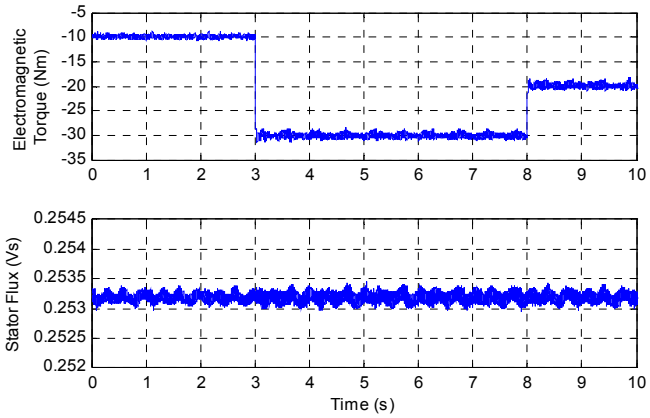

Fig. 15. The dynamic responses of torque and stator flux magnitude of PMSG #2 using the proposed DTC.

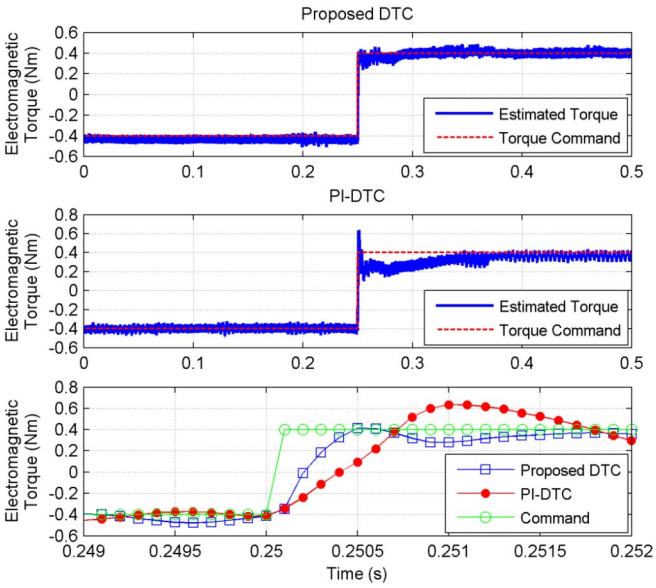

Fig. 16. The transient performances of the PMSG #1 controlled by the proposed DTC and the PI-DTC under a complete torque reversal.

Fig. 16 compares the torque tracking performances of PMSG #1 controlled by the proposed DTC and the PI-DTC under a complete torque reversal from −0.4 N·m to 0.4 N·m (80% rated torque), where PMSG #1 is operated at 2000 RPM, the reference of the stator flux magnitude is 0.0135 V·s, the torque command is changed within one step at 0.25 s, the PI gains of the PI-DTC are the same as those used in the test shown in Fig. 14. The curves in the bottom plot are obtained by zooming in the curves in the two top plots in a much smaller time interval to show clearly how the torque changes in each control cycle. As shown in the figure, the estimated actual torques and the torque command are on top of each other during the steady-state operation for both methods. However, when the PI-DTC is used, an obvious overshoot is observed during the transient; and it takes 7 switching cycles (0.7 ms) and 100 ms for the torque to track its reference and settle down to the steady state, respectively. Compared to the PI-DCT, the proposed DTC controls the PMSG to achieve the complete torque reversal within 5 switching cycles without any overshoot and settle down to the steady state within 1.5 ms. The result shows that a much faster transient response is

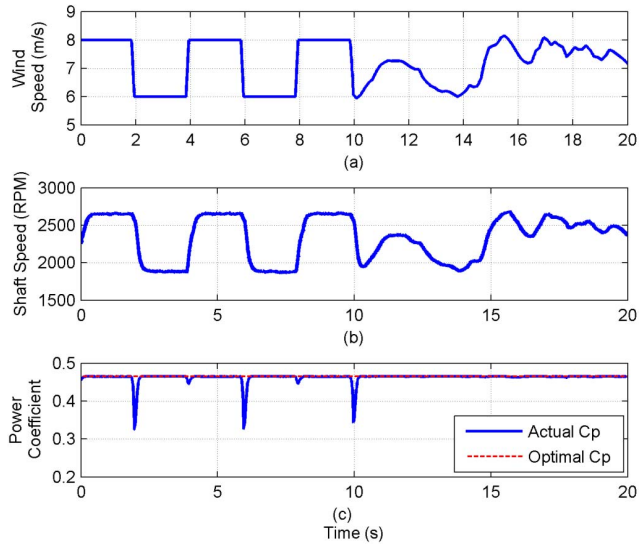

Fig. 17. The dynamic performance of the PMSG #1-based direct-drive WECS controlled by the proposed DTC: (a) wind speed, (b) shaft speed, and (c) actual and optimal power coefficients.

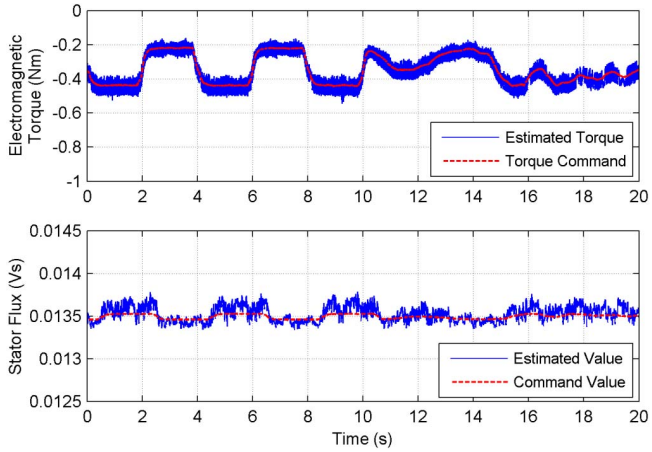

Fig. 18. The electromagnetic torque and stator flux responses of the PMSG #1-based direct-drive WECS controlled by the proposed DTC.

obtained by using the proposed DTC than the PI-DTC in a different operating condition. Moreover, compared to the PI-DTC, the proposed DTC removes the tedious process of tuning PI gains. Although the transient of the active flux in (25) is neglected, the proposed DTC can still attain fast dynamic response when the controlled PMSG has saliency.

Finally, the proposed DTC is applied to PMSG #1 to emulate the operation of a direct-drive WECS, where the DC motor is controlled to emulate the dynamics of a real wind turbine. As shown in Fig. 17(a), the wind speed profile used in this test consists of two parts. In the first 10 seconds, the wind speed changes alternatively between 6 m/s and 8 m/s. The frequency of the periodic wind speed variations is 0.25 Hz. The slew rate of the wind speed changes is 20 $m \cdot s^{-1}/s$. The wind speed profile in Fig. 11(a) is adopted for the second 10 seconds. The wind speed data is shrank to [5.8, 8.2] m/s to match the operating range of the emulated wind turbine. The torque command for PMSG #1 is given by (32), where K_{opt} is calculated as $5.6553 \cdot 10^{-6}$ based on the parameters of the emulated wind turbine. The command of stator flux magnitude

0093-9994 (c) 2015 IEEE. Personal use is permitted, but republication/redistribution requires IEEE permission. See http://www.ieee.org/publications_standards/publications/rights/index.html for more information.

This article has been accepted for publication in a future issue of this journal, but has not been fully edited. Content may change prior to final publication. Citation information: DOI 10.1109/TIA.2015.2413760, IEEE Transactions on Industry Applications

is obtained from the principle of MTPA as well. The dynamic responses of the shaft speed and the actual and optimal power coefficients are shown in Fig. 17(b) and (c), respectively. The actual power coefficient of the WECS approaches the optimal value closely. Due to the moment of inertia of the system, the shaft speed cannot be varied abruptly when sudden wind speed changes occurred. However, the actual power coefficient can keep tracking the optimal value within 0.2 seconds. Fig. 18 shows the tracking performance of the electromagnetic torque and the stator flux magnitude. With the proposed DTC, the estimated torque and stator flux magnitude and their commands are always on top of each other. The peak-to-peak torque and stator flux magnitude ripples are less than 0.1 N·m (8% of the maximum torque) and 0.0004 V·s (3% of the base flux magnitude), respectively. Moreover, the torque and stator flux magnitude tracking performance of the PMSG controlled by the proposed DTC is not deteriorated under load and speed variations.

VI. Conclusion

This paper has proposed a novel discrete-time DTC based on flux space vectors for PMSGs used in direct-drive WECSs. The algorithm is easy to implement and is suitable for digital control systems using relatively low sampling frequencies. The torque and flux ripples have been significantly reduced with the integration of the SVM. In addition, the overall DTC scheme eliminated the use of PI controllers, showed strong robustness to machine parameter variations, and achieved fast dynamic responses. The proposed DTC scheme can be applied to both nonsalient-pole and salient-pole PMSGs. Simulation and experimental results have been carried out to validate the effectiveness of the proposed DTC scheme on a 180 W salient-pole PMSG and nonsalient-pole PMSG used in a 2.4 kW Skystream 3.7 direct-drive WECS.

Appendix

According to (7), the derivative of electromagnetic torque with respect to load angle can be derived as

$$\frac{dT_e}{d\delta}=\frac{3}{2}\frac{n}{L_d}|\psi_s|\left(\psi_m\cos\delta+|\psi_s|\frac{(L_d-L_q)}{L_q}\cos(2\delta)\right)>0. \quad \text{(A-1)}$$

For the nonsalient-pole PMSGs ($L_d = L_q$), the stable operating region of δ is within ($-\pi/2$, $\pi/2$). If $L_d \neq L_q$, (A-1) can be simplified as

$$2a(\cos\delta)^2-b\cos\delta-a<0,\qquad a=\frac{L_q-L_d}{L_q},b=\frac{\psi_m}{|\psi_s|}. \quad \text{(A-2)}$$

where a and b are both positive coefficients. The solution to (A-2) can be derived as

$$\frac{b-\sqrt{b^2+8a^2}}{4a}<\cos\delta<\frac{b+\sqrt{b^2+8a^2}}{4a}. \quad \text{(A-3)}$$

Therefore, the maximum load angle for a salient-pole PMSG is

$$\delta_{\max}=\arccos\left(\frac{b-\sqrt{b^2+8a^2}}{4a}\right). \quad \text{(A-4)}$$

Equation (A-4) indicates that δ_{max} exceeds $\pi/2$ since $(b-\sqrt{b^2+8a^2})/(4a)<0$. On the other hand, the inequality $(b+\sqrt{b^2+8a^2})/(4a)>1$ should be satisfied in order for the PMSG to be operated stably within $[-\delta_{max}, \delta_{max}]$. Solving the inequality yields

$$|\psi_s|<\frac{L_q}{L_q-L_d}\psi_m. \quad \text{(A-5)}$$

References

[1] Y. Zhao, C. Wei, Z. Zhang, and W. Qiao, "A review on position/speed sensorless control for permanent-magnet synchronous machine-based wind energy conversion systems," *IEEE J. Emerging and Selected Topics in Power Electron.*, vol. 1, no. 4, pp. 203-216, Dec. 2013.

[2] W. Qiao, L. Qu, and R. G. Harley, "Control of IPM synchronous generator for maximum wind power generation considering magnetic saturation," *IEEE Trans. Ind. Appl.*, vol. 45, no. 3, pp. 1095-1105, May/Jun. 2009.

[3] W. Qiao, X. Yang, and X. Gong, "Wind speed and rotor position sensorless control for direct-drive PMG wind turbines," *IEEE Trans. Ind. Appl.*, vol. 48, no. 1, pp. 3-11, Jan./Feb. 2012.

[4] "Direct torque control–The world's most advanced AC drive technology," ABB, Tech. Guide No. 1. Jun. 2011.

[5] Z. Zhang, Y. Zhao, W. Qiao, and L. Qu, "A space-vector modulated sensorless direct-torque control for direct-drive PMSG wind turbines," *IEEE Trans. Ind. Appl.*, vol. 50, no. 4, pp. 2331-2341, Jul./Aug. 2014.

[6] L. Zhong, M. F. Rahman, W. Y. Hu, and K. W. Lim, "Analysis of direct torque control in permanent magnet synchronous motor drives," *IEEE Trans. Power Electron.*, vol. 12, no. 3, pp. 528-536, May. 1997.

[7] C. A. Martins, X. Roboam, T. A. Meynard, and A. S. Carvalho, "Switching frequency imposition and ripple reduction in DTC drives by using a multilevel converter," *IEEE Trans. Power Electronics*, vol. 17, no. 2, pp. 286- 297, Mar. 2002.

[8] Y. Zhang, J. Zhu, Z. Zhao, W. Xu, and D. G. Dorrell, "An improved direct torque control for three-level inverter-fed indution motor sensorless drive," *IEEE Trans. Power Electronics*, vol. 27, no. 3, pp. 1502- 1513, Mar. 2002.

[9] D. Casadei, F. Profumo, and G. Serra, "FOC and DTC: Two viable schemes for induction motors torque control," *IEEE Trans. Power Electronics*, vol. 17, no. 5, pp. 779- 787, Sept. 2002.

[10] G. S. Buja and M. P. Kazmierkowski, "Direct torque control of PWM inverter-fed AD motors – A survey," *IEEE Trans. Ind. Electron.,* vol. 42, no. 4, pp. 344–350, Aug. 1995.

[11] T. G. Habetler, F. Profumo, M. Pastorelli, and L. M. Tolbert, "Direct torque control of induction machines using space vector modulation," *IEEE Trans. Ind. Appl.*, vol. 28, no. 5, pp. 1045-1053, Sept./Oct. 1992.

[12] I. Boldea, M. C. Paicu, G. D. Andreescu and F. Blaabjerg, "'Active flux' DTFC-SVM sensorless control of IPMSM," *IEEE Trans. Energy Conversion*, vol. 24, no. 2, pp. 314- 322, Jun. 2009.

[13] M. C. Paicu, I. Boldea, G. D. Andreescu, and F. Blaabjerg, "Very low speed performance of active flux based sensorless control: Interior permanent magnet synchronous motor vector control versus direct torque and flux control," *IET Electric Power Application*, vol. 3, no. 6, pp. 551-561, Nov. 2009.

[14] Y. Lai, and J. Chen, "A new approach to direct torque control of induction motor drives for constant inverter switching frequency and torque ripple reduction," *IEEE Trans. Energy Conversion*, vol. 16, no. 3, pp. 220-227, Sept. 2001.

[15] M. Fu and L. Xu, "A sensorless direct torque control technique for permanent magnet synchronous motors," in *Proc. IEEE IAS Annu. Meeting*, May 1999, vol. 1, pp. 159-164.

[16] M. Pacas and J. Weber, "Predictive direct torque control for the PM synchronous machine," *IEEE Trans. Ind. Electron.*, vol. 52, no. 5, pp. 1350-1356, Oct. 2005.

[17] H. Moon, H. Kim, and M.Youn, "A discrete-time predictive current control for PMSM," *IEEE Trans. Power Electron.*, vol. 18, no. 1, pp. 464-472, Jan. 2003.

[18] J. Lee, C. Choi, J. Seok, and R.D. Lorenz, "Deadbeat-direct torque and flux control of interior permanent magnet synchronous machines with

0093-9994 (c) 2015 IEEE. Personal use is permitted, but republication/redistribution requires IEEE permission. See http://www.ieee.org/publications_standards/publications/rights/index.html for more information.

This article has been accepted for publication in a future issue of this journal, but has not been fully edited. Content may change prior to final publication. Citation information: DOI 10.1109/TIA.2015.2413760, IEEE Transactions on Industry Applications

discrete time stator current and stator flux linkage observer," *IEEE Trans. Ind. Appl.* vol. 47, no. 4, pp. 1749-1758, Jul.-Aug. 2011.

[19] M. Shin, D. Hyun, S. Cho, and S. Choe, "An improved stator flux estimation for speed sensorless stator flux orientation control of induction motors," *IEEE Trans. Power Electron.*, vol. 15, no. 2, pp. 312-318, Mar. 2000.

[20] S. Morimoto, H. Nakayama, M. Sanada, and Y. Takeda, "Sensorless output maximization control for variable-speed wind generation system using IPMSG," *IEEE Trans. Ind. Appl.*, vol. 41, no. 1, pp. 60-67, Jan/Feb. 2005.

[21] I. Boldea, M. C. Paicu, and G. D. Andreescu, "Active flux concept for motion-sensorless unified AC drives," *IEEE Trans. Power Electron.*, vol. 23, no. 5, pp. 2612- 2618, Sept. 2008.

[22] Y. Zhao, W. Qiao, and L. Wu, "Dead-time effect and current regulation quality analysis for a sliding-mode position observer-based sensorless IPMSM drives," *IEEE Trans. Ind. Appl.,* in press. (Available online in IEEE Xplore)

[23] Y. Zhang, J. Zhu, W. Xu, and Y. Guo, "A simple method to reduce torque ripple in direct torque-controlled permanent-magnet synchronous motor by using vectors with variable amplitude and angle," *IEEE Trans. Ind. Electron.,* vol. 58, no. 7, pp. 2848- 2859, Jul. 2011.

[24] W. Qiao, W. Zhou, J. M. Aller, and R. G. Harley, "Wind speed estimation based sensorless output maximization control for a wind turbine driving a DFIG," *IEEE Trans. Power Electron.,* vol. 23, no. 3, pp. 1156- 1169, May 2008.

Zhe Zhang (S'10) received a B.S. degree in electrical engineering from Xi'an Jiaotong University, Xi'an, China, in 2010. Currently, he is working toward a Ph.D. degree in electrical engineering at the University of Nebraska—Lincoln, Lincoln, NE, USA.

He worked as an electrical engineering intern at Rockwell Automation in summer 2014. His current research interests include control of wind energy conversion systems, power electronics, and motor drives.

Yue Zhao (S'10–M'14) received a B.S. degree in electrical engineering from Beijing University of Aeronautics and Astronautics, Beijing, China, in 2010, and a Ph.D. degree in electrical engineering from the University of Nebraska—Lincoln (UNL), Lincoln, NE, USA, in 2014.

He was a product engineering intern with John Deere Electronic Solutions, Fargo, ND, in 2013 and an electrical engineering intern with Nexteer Automotive, Saginaw, MI, in 2014. Since August 2014, he has been with the Virginia Commonwealth University, USA, where he is currently an Assistant Professor in the Department of Electrical and Computer Engineering. His current research interests include electric machines and drives, power electronics, and renewable energy systems. He is the coinventor of 4 U.S. patents pending in electric motor drives and the coauthor of more than 20 papers in refereed journals and international conference proceedings.

Dr. Zhao is a member of Eta Kappa Nu. He was a recipient of the Best Paper Prize of the 2012 IEEE Transportation Electrification Conference and Expo and the recipient of the 2014 UNL Outstanding Graduate Research Assistant (GRA) Award.

Wei Qiao (S'05–M'08–SM'12) received the B.Eng. and M.Eng. degrees in electrical engineering from Zhejiang University, Hangzhou, China, in 1997 and 2002, respectively, the M.S. degree in high performance computation for engineered systems from Singapore-MIT Alliance (SMA), Singapore, in 2003, and the Ph.D. degree in electrical engineering from Georgia Institute of Technology, Atlanta, GA, USA, in 2008.

Since August 2008, he has been with the University of Nebraska—Lincoln (UNL), USA, where he is currently an Associate Professor in the Department of Electrical and Computer Engineering. His research interests include renewable energy systems, smart grids, microgrids, condition monitoring and fault diagnosis and prognosis, energy storage systems, power electronics, electric machines and drives, and computational intelligence. He is the author or coauthor of 3 book chapters and more than 150 papers in refereed journals and international conference proceedings and has 6 international/U.S. patents pending.

Dr. Qiao is an Editor of the IEEE Transactions on Energy Conversion, an Associate Editor of IET Power Electronics and the IEEE Journal of Emerging and Selected Topics in Power Electronics, and the Corresponding Guest Editor of a special section on Condition Monitoring, Diagnosis, Prognosis, and Health Monitoring for Wind Energy Conversion Systems of the IEEE Transactions on Industrial Electronics. He was an Associate Editor of the IEEE Transactions on Industry Applications in 2010-2013. He was the recipient of a 2010 U.S. National Science Foundation CAREER Award, the 2010 IEEE Industry Applications Society (IAS) Andrew W. Smith Outstanding Young Member Award, the 2012 UNL College of Engineering Faculty Research & Creative Activity Award, the 2011 UNL Harold and Esther Edgerton Junior Faculty Award, and the 2011 UNL College of Engineering Edgerton Innovation Award. He has received four best paper awards from IEEE IAS, PES, and PELS.

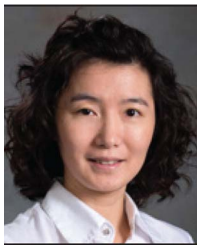

Liyan Qu (S'05–M'08) received the B.Eng. (with the highest distinction) and M.Eng. degrees in electrical engineering from Zhejiang University, Hangzhou, China, in 1999 and 2002, respectively, and the Ph.D. degree in electrical engineering from the University of Illinois at Urbana–Champaign, USA, in 2007.

From 2007 to 2009, she was an Application Engineer with Ansoft Corporation. Since January 2010, she has been with the University of Nebraska—Lincoln (UNL), where she is currently an Assistant Professor in the Department of Electrical and Computer Engineering. Her research interests include energy efficiency, renewable energy, numerical analysis and computer aided design of electric machinery and power electronic devices, dynamics and control of electric machinery, permanent-magnet machines, and magnetic materials.

0093-9994 (c) 2015 IEEE. Personal use is permitted, but republication/redistribution requires IEEE permission. See http://www.ieee.org/publications_standards/publications/rights/index.html for more information.